Modeling and thermal management of proton exchange membrane fuel cell for fuel cell/battery hybrid automotive vehicle

Lu Xing[a], Wentao Xiang[b], Runqi Zhu[c], Zhengkai Tu[b,*]

[a] Mechanical and Construction Engineering, Northumbria University, Newcastle upon Tyne, NE1 8ST, United Kingdom

[b] School of Energy & Power Engineering, Huazhong University of Science & Technology, Wuhan, 430074, China

[c] China-EU Institute for Clean and Renewable Energy, Huazhong University of Science & Technology, Wuhan, 430074, China

*Corresponding author: tzklq@hust.edu.cn

Abstract

The proton exchange membrane fuel cell (PEMFC) stack is a key component in the fuel cell/battery hybrid vehicle. Thermal management and optimized control of the PEMFC under real driving cycle remains a challenging issue. This paper presents a new hybrid vehicle model, including simulations of diver behavior, vehicle dynamic, vehicle control unit, energy control unit, PEMFC stack, cooling system, battery, DC/DC converter, and motor. The stack model had been validated against experimental results. The aim is to model and analyze the characteristics of the 30 kW PEMFC stack regulated by its cooling system under actual driving conditions. Under actual driving cycles (0-65kW/h), 33% to 50% of the total energy becomes stack heat; the heat dissipation requirements of the PEMFC stack are high and increase at high speed and acceleration. A PID control is proposed; the cooling water flow rate is adjusted; the control succeeded in stabilizing the stack temperature at 350K at actual driving conditions. Constant and relative lower inlet cooling water temperature (340K) improves the regulation ability of the PID control. The hybrid vehicle model can provide a theoretical basis for the thermal management of the PEMFC stack in complex vehicle driving conditions.

Keywords: Automotive vehicle; Battery; PID regulator; Proton exchange membrane fuel cell; Vehicle integrated thermal management

1 Introduction

Fuel cell (FC) is a high-efficiency power generation device that directly converts the chemical energy of fuel and oxidant (often oxygen) into electrical energy through electrochemical reactions. Proton exchange membrane fuel cell (PEMFC) has a low operating temperature (60~80°C), good stability, high energy density, non-corrosive electrolyte; it is suitable for use as automobile engines for fuel cell/battery hybrid vehicles [1-4]. However, the heat dissipation of the PEMFC stack is much more complicated than the one of the traditional internal combustion engines.

The heat dissipation of traditional internal combustion engines is mainly through the engine body and exhaust gas, while it is not so for the fuel cell stack. The fuel cell stack is generally well-insulated; more than 95% of the heat needs to be dissipated through the coolant. Therefore, the thermal load of a fuel cell vehicle is even twice that of a traditional vehicle. This leads to a high requirement for the performance of the thermal management system for the PEMFC stack [5,6]. Moreover, the thermal management system is required to ensure the uniformity of the temperature distribution of the fuel cell stack to prevent the proton exchange membrane from being exposed to unfavorable temperature and humidity environments [7,8]. Under actual driving cycles, temperature changes in the stack are considerably more significant, which cause thermal stresses and material degradation. At actual driving conditions, the thermal management and control of the PEMFC stack, which plays a crucial role in efficiency optimization, lifetime extension, and operational safety, is essential for the fuel cell/battery hybrid vehicle [9-12].

There was research that focused on the performance of the fuel cell at start-stop conditions. Zhang et al. [13] analyzed and discussed the gas distribution process in the fuel cell during start-stop, leading to degradation. Meier et al. [14] studied the degradation of the fuel cell catalyst under simulated start-stop conditions. Pahon et al. [15] evaluated the degradation behavior of fuel cell during and proposed a shutdown strategy. Rabbni et al. [16] established a control-oriented fuel cell system model with all necessary auxiliary components. The simulation results under the startup scenario show that the system is more efficient when starting at low power, but it takes longer for the stack to reach a steady state. Cheng et al. [17] established a PEMFC urban bus model based on experimental data and proposed a three-step preheating scheme. The simulation results reveal that a longer warm-up time and higher ambient temperature can improve the system's efficiency. Wang et al. [18] investigated the cold start strategies for the PEMFCs and concluded that improving fuel cell materials' thermal conductivity is critical for startup success.

Under actual driving conditions, few scholars researched the energy management of fuel cell vehicles [19]. Zhou et al. [20] developed a simulation model for a medium-sized plug-in fuel cell/battery hybrid electric vehicle and proposed a multi-criteria energy distribution strategy. The energy management system under this strategy can reduce hydrogen consumption by more than 12.1% while significantly reducing the average transient power of the battery. Andari et al. [21] developed a fuel cell/supercapacitor vehicle simulation model. They proposed a simplified energy management model based on supercapacitor state of charge (SOC) and driving mode.

The model simulates the system characteristics under the New European Driving Cycle (NEDC) operating conditions and obtains the hydrogen consumption curve. Wang et al. [22] developed a finite state machine-based energy management strategy for the battery/fuel cell and battery/supercapacitor/fuel cell system to maximize the fuel cell output net power. Zhang et al. [23] proposed a power management strategy to enhance onboard fuel cell durability for fuel cell plug-in hybrid vehicles. Kaya and Hames [24] examined two control strategies for hydrogen fuel-saving and to extend the life cycle in the battery/supercapacitor/fuel cell vehicle. Zeng et al. [25] proposed an optimization-oriented adaptive equivalent consumption minimization strategy for fuel cell hybrid vehicles, which can quickly recover the battery state of charge within 40 s in a 500-s driving cycle. Zhang et al. [26] suggested a short-term speed prediction method for analyzing the future energy consumption of intelligent fuel cell vehicles.

Few researchers investigated the impact of aging and thermal management of a fuel cell on energy management strategies for fuel cell vehicles. Kandidayeni et al. [27] proposed a rule-based energy management system based on studies of two significant aspects, fuel cell degradation, and thermal management. Zhou et al. [28] designed cost-minimization energy management for the fuel cell electric vehicle, both fuel consumption and degradation are considered. Li et al. [29] suggested a consumption minimum strategy for fuel cell hybrid electric vehicles that considers the power source's degradation. The thermal management system model was simplified for these studies.

Researchers explored the influence of different factors on PEMFC heat dissipation and thermal management system and suggested optimization schemes and improvement

strategies [30]. Liso et al. [31] proposed a liquid-cooled PEMFC system dynamic model to study temperature changes caused by rapid load changes. It is found that slow temperature control will affect the system's stability, so a feed-forward control strategy is adopted. Islam et al. [32] suggested 2% nanofluid can obtain 63% convective heat transfer enhancement, meanwhile, no significant difference was found in pumping power. Bargal et al. [33] presented the ZnO, and ALN nanofluid coolant contribute to enhancing the heat transfer and radiator cooling effectiveness for automotive PEMFC applications. Zhang et al. [34] combined a one-dimensional PEMFC engine simulation model with radiator fan models to study the heat dissipation characteristics of the PEMFC cooling system, considering the model accuracy and simulation time. The simulation results prove that the thermal management system can maintain a suitable temperature in a relatively high-temperature environment. Han et al. [35] paid attention to the impact of ram air compensation on the cooling system. They adopted three different driving cycle conditions to test the effect of ram air on the cooling system performance and get the optimal control strategy. Sun et al. [36] designed and modeled a waste heat reuse system for the 60kW fuel cell vehicle.

In these proposed models, fuel cell stack model was not integrated with a whole vehicle model. Previous studies barely investigate the thermal balance and performance of the fuel cell stack under actual driving conditions. The impact of changing driving conditions on the PEMFC stack's performance and the cooling system's operation needs further investigation. Liang et al. [37] discussed advances and challenges of integrated thermal management technologies for electric vehicles. Lu et al. [38] suggested a model

predictive control for integrated vehicle thermal management for electric cars; the engine compartment was described with the lumped parameter method. Wang et al. [39] constructed a thermal management model for a 100kW full-powered fuel cell vehicle. Zhao et al. [40] developed and investigated a novel vehicle integrated thermal management system with a heat-pump system for waste heat re-use of the fuel cell vehicles. Xu et al. [41] modeled a vehicle integrated thermal management system for fuel cell sport utility vehicles. The vehicle is powered by a 36 kW PEMFC stack and 11 kW Li-ion battery. A vehicle dynamic model and motor model is developed. The paper analyzes heat generation and transfer of PEMFC, also motor, and other components.

In this paper, a comprehensive model of vehicle integrated thermal management system has been developed to analyze the performance of PEMFC stack for the fuel cell/battery hybrid vehicle. A PID controller is proposed for regulating the thermal balance of the stack under actual driving conditions. The cooling water flow rate is adjusted to stabilize the stack temperature. We simulated and studied the dynamic characteristics of the heat dissipation capability of the PEMFC cooling system under the PID control.

2 System description

There are four energy configurations for the fuel cell vehicles: full fuel cell (FC) vehicle, fuel cell, and battery (FC+B) hybrid vehicle, fuel cell and ultra-capacitor (FC+C) hybrid vehicle, vehicle mixed with fuel cell, battery, and ultra-capacitor (FC+B+C) [42]. The FC vehicle only uses FC stack as an energy supply without any other auxiliary power source. This type is usually applied to low-speed vehicles such as forklifts, buses, and

so on. FC+B vehicle is the most common hybrid energy form, for its battery units enabling FC operating at high-efficiency zone. FC+C structure replaces the battery units with ultra-capacitor to satisfy the transient power demand, though ultra-capacitor cannot supply energy continuously due to their low energy density. FC+B+C vehicle is proposed to provide continuous energy and enhance the dynamic response of FC during transient events [11]. Due to the limitation of the fuel cell load changing performance, hybrid vehicles have more tremendous advantages. With high specific power and more energy storage, the cruising range of fuel cell electric vehicles is significantly increased.

Through parameter studies, Bauman et al. [43] compared the FC+B, FC+C, and FC+B+C hybrid vehicles. They included the acceleration time, fuel economy and cost in the objective function and concluded that FC + C configuration is the least ideal. FC + B and FC + B + C configurations are close competitors. Changizian et al. [44] found that when compared with FC+B, the FC + B + C allows for 3.3% reduction in fuel consumption based on three cycle simulations. However, FC + B hybrid vehicle is generally less costly. Thus, the FC+B configuration is chosen for this study [45]. In the "FC+B" model, the lithium battery provides peak current for the high-power behavior of the vehicle during driving; it also uses a kinetic energy recovery system to reduce fuel consumption.

The schematic diagram of the FC+B hybrid vehicle model is shown in Fig. 1. The fuel supply system delivers the hydrogen and air to the fuel cell, the car's primary power source. The battery is an auxiliary power source that provides peak current and absorbs

the braking energy. Its current with the current generated by the FC engine is fed to the motor controller through the DC/DC converter, which controls the operation of the motor. The motor rotates the wheels by the transmission system. The following section provides a detailed description of each component's modeling method and the relationship of the component models.

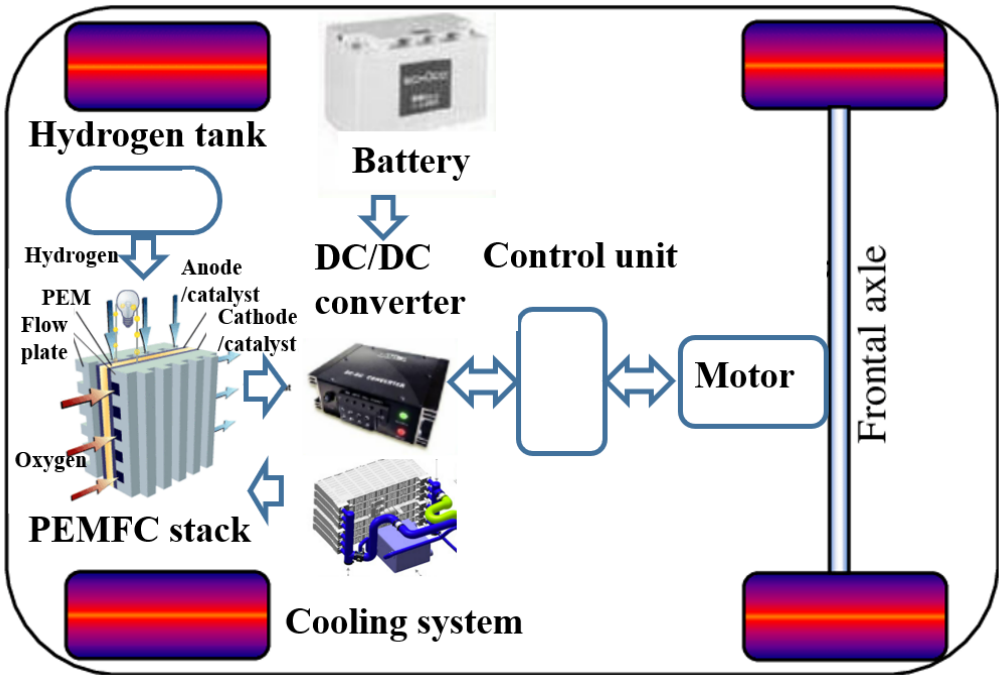

Figure 1: Fuel cell + Battery hybrid vehicle

2.1 Hybrid vehicle model

Hybrid vehicle model includes simulations of few subsystems, such as dynamic system, control system, PEMFC system, battery system, DC/DC converter, and motor. The flow chart of the hybrid vehicle model is shown in Fig. 2. The control system receives data from the dynamic system, makes judgments, feeds the corresponding demand signals to the PEMFC system and battery system, and controls the motor. Under actual driving conditions, the hybrid vehicle model simulates the changing energy demands from the

PEMFC system decided by the control system. This paper focuses on the PEMFC stack's performance and cooling system to satisfy the changing energy demands. We studied the dynamic characteristics, analyzed the impact of variations of water flow rate and stack inlet cooling water temperature on the cooling system performance. A PID controller is proposed for optimizing the performance of the PEMFC stack.

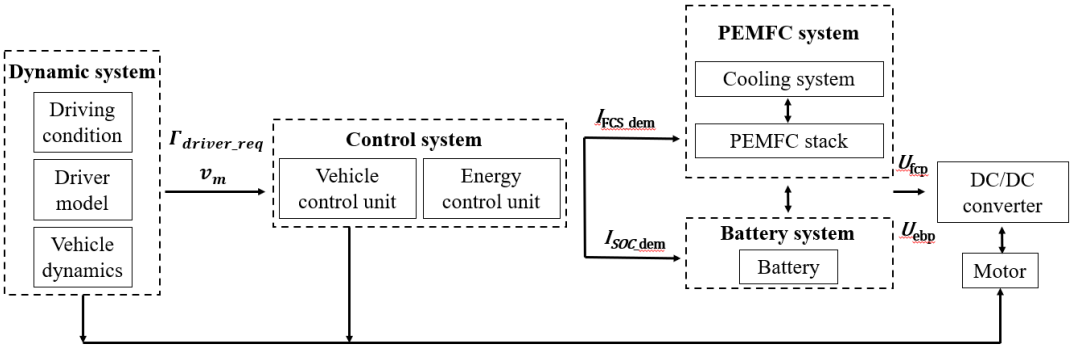

Figure 2: Hybrid vehicle model flow chart

2.2 Dynamic system

The driving condition is a function of time and vehicle speed, including important road condition information such as the average speed of the vehicle, the maximum speed, and the acceleration ratio. The latest China automotive test cycle (CLTC-P, Standard GB/T 38146.1-2019) is used as the input data. The driving condition has a total duration of 1800s, and the working condition curve is shown in Fig. 3. The driving conditions of Chinese passenger cars include low, medium, and high-speed zones. The low-speed zone is from 0 to 674 seconds, the medium-speed zone is from 674 to 1367 seconds, and the high-speed zone is from 1367 seconds to 1800 seconds.

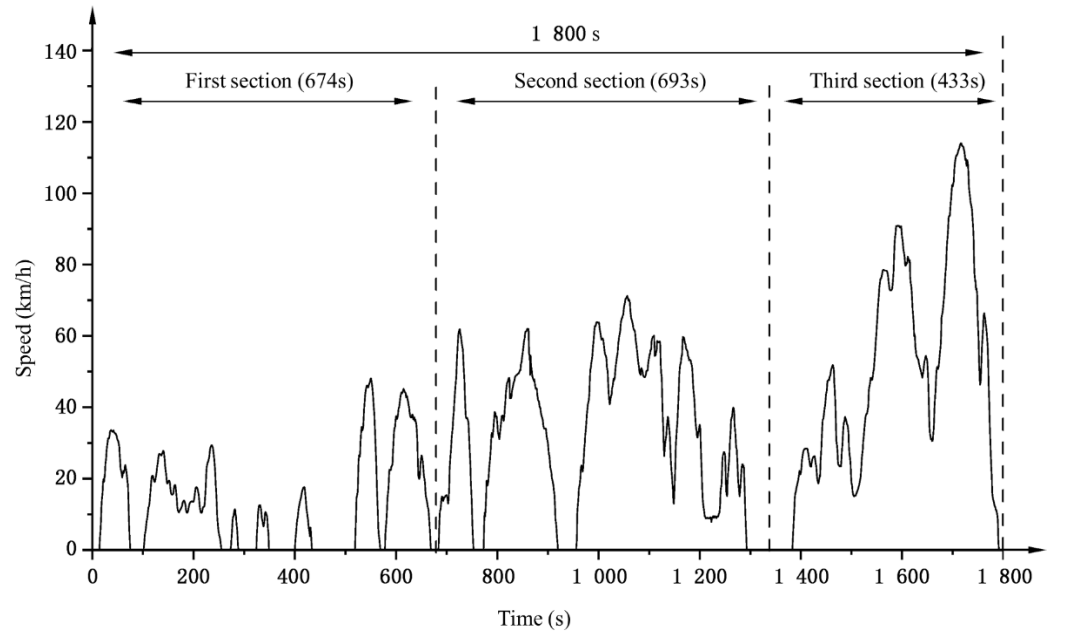

Figure 3: Reference vehicle speed - China automotive test cycle

2.2.1 Driver model

The reference speed presented in Fig. 3 will be the input for the driver model. The driver model is an important part of the hybrid vehicle model. The model simulates the driver's perception and operation of actual road conditions and transmits the operating signals to the corresponding actuators of the vehicle. Traditional driver models are often based on classic control theory. A PID regulator is used to simulate driver behavior through the proportional, differential, and integral to control the speed error and acceleration, as presented in Equations (1) – (3):

$$\Delta v = v_{ref} - v_m \tag{1}$$

$$\Gamma_{driver\_req} = k_p \Delta v + \Gamma_i + k_d \frac{dv_m}{dt} \tag{2}$$

$$\dot{\Gamma}_i = k_i(\Delta v - k_a \Gamma_i) \tag{3}$$

Where, v_{ref} is the reference vehicle speed of the driving condition (m/s). v_m is the actual vehicle speed sent by the vehicle dynamic model (m/s). Γ_{driver_req} is the driver's

reference torque (N·m) which will be used as input for the control system. The four parameters of k_p、k_d、k_i、k_a are determined by minimizing the difference of the actual vehicle speed and the reference vehicle speed.

2.2.2 Vehicle dynamic model

The vehicle dynamic model processes the vehicle environmental parameters, braking torque Γ_{brake}, transmission system output torque Γ_{wheel} and motor equivalent moment of inertia Θ_{motor}, calculates actual vehicle speed v_m, wheel angular velocity ω_{wheel} and vehicle acceleration a_m. The proposed model only focuses on the force of the vehicle in the driving direction. The vehicle model is based on Newtonian dynamic equations. When the torque generated by the engine acts on the wheel, the wheel has a force on the ground, this is the driving force F_Γ of the car, as shown in Equation (4):

$$F_\Gamma = \frac{\Gamma}{r} \tag{4}$$

Where, r (m) is the static radius of the tire (m), and Γ is the engine torque (N·m), the change in the wheel radius during the car driving is neglected. Vehicle resistance includes rolling resistance, air resistance, gradient resistance, and acceleration resistance, as shown in Equations (5) – (8) [22-24, 29]:

$$F_f = f\, mgcos\, \alpha \tag{5}$$

$$F_{air} = \frac{\rho}{2} \cdot C_D \cdot A_{veh} \cdot v^2 \tag{6}$$

$$F_i = mg\, sin\, \alpha \tag{7}$$

$$F_a = \delta m \frac{dv}{dt} \tag{8}$$

Where, f is the rolling resistance coefficient. m is the vehicle mass (kg), C_D is the air resistance coefficient. A_{veh} is the windward area of the car (m^2). ρ is the air density

(kg/m^3). α is gradient angle. δ is the conversion coefficient of car rotation mass. The tire rolling resistance coefficient is related to the driving speed. When the driving speed increases, the tire rolling resistance will continue to decrease. The rolling resistance coefficient also depends on the material of the tire and the road surface. We use Newton's second law to establish dynamic equations, as shown in Equation (9):

$$\dot{\omega}_{wheel} = \frac{(F_\Gamma + F_{brake} + F_{res}) \cdot r}{\Theta_{motor} + \Theta_{wheel} + mr^2} \quad (9)$$

Where, $\dot{\omega}_{wheel}$ is the angular acceleration (s^{-2}). F_{brake} is the resistance due to brake, output from the control system(N). F_{res} is the sum of all driving resistance (N). Θ_{motor} is the equivalent moment of inertia of the motor (kg·m^2), calculated from the motor model. Θ_{wheel} is the moment of inertia of the wheel (kg·m^2). mr^2 is the moment of inertia of the body (kg·m^2). The actual velocity v_m can be calculated from the angular acceleration $\dot{\omega}_{wheel}$. The parameters in this model are adopted from [46], shown in Table 1.

Table 1: Vehicle parameters

Parameter (unit)	Value
Vehicle mass m (kg)	1653
Air resistance coefficient C_D (-)	0.32
Windward area A_{veh} (m^2)	2.42
Tire radius r (m)	0.2946
The moment of inertia of wheel Θ_{wheel} (kg·m^2)	3.2
The moment of inertia of the motor Θ_{motor} (kg·m^2)	0.1098
Ambient temperature T_{amb} (°C)	20

2.3 Control system

2.3.1 Vehicle control unit

Vehicle control unit (VCU) modeling including two aspects: (a) Based on the driver's reference torque signal of the driver model and the actual speed signal of the vehicle dynamic model, and judge the operating mode, whether it is at motor operating mode, the generator operating mode or the idling condition. (b) Calculate the corresponding motor demand torque, motor demand current (output to the energy control unit), and braking demand torque for the decided operating mode.

2.3.2 Energy control unit

An energy control unit (ECU) is required to control the energy flow of the vehicle. The primary power source of the hybrid vehicle is the PEMFC, and the auxiliary power source is the battery. When the vehicle is accelerating or climbing, the required output power of the vehicle is relatively large; the battery system provides a part of the power to prevent the PEMFC output power from being too high. When the vehicle starts to brake, the car's kinetic energy is converted into electric energy and stored in the battery through the generator mode. In addition, when the state of charge (SOC) is insufficient, the PEMFC engine can also provide electric energy. It is assumed to be an ideal process; the battery can store all excess FC stack energy.

The strategy of the energy control unit must achieve two goals: (a) It must be able to reasonably set the power source device (PEMFC and battery) and the dynamic device (motor and wheels) to meet the needs and constraints of driving. (b) To achieve the optimization through the energy control strategy, such as fuel consumption and lifetime. This paper focuses on investigating the heat dissipation capacity of the fuel cell engine

under actual operating conditions; a regular control strategy is proposed, optimization of vehicle power performance and the economy is not considered. The regular control strategy mainly includes simulations of four modules: the fuel cell system (FCS) start-stop control module, the motor operating mode module, the generator operating mode module, and the idling operating mode module. The input signal of the FCS start-stop control module is the actual vehicle speed signal, and the output is the FCS switch signal. The control logic is to turn off the engine when the car brakes (the vehicle's actual speed is greater than 0, and the actual acceleration of the vehicle is less than 0). In other cases, the FCS is turned on. Then, according to the vehicle operating mode and the FCS status signal, the ECU calculates the corresponding FCS demand current I_{FCS_dem}, battery demand current I_{soc_dem}, and DC/DC converter demand current I_{hvp_dem}.

2.4 Proton exchange membrane fuel cell system

2.4.1 PEMFC stack

The PEMFC stack is a critical part of the hybrid vehicle. The fuel cell comprises reactive electrodes, gas diffusion layers, proton exchange membranes, and catalytic layers. Hydrogen fuel and oxygen enter the anode and cathode, respectively. On the anode, hydrogen reacts (with the presence of the catalyst) to generate ions and electrons. The ions move through the membrane to reach the cathode. The electrons move on the external circuit. The oxygen on the cathode reacts with the ions and electrons and generates electricity and water. The mathematical relationship between stack power, heat production and various parameters can be obtained to establish the PEMFC stack model. The output voltage of fuel cell can be calculated from Equation (10):

$$V_{FC} = V_{Nernst} - V_{act} - V_{ohm} - V_{con} \quad (10)$$

Where, V_{Nernst} is the Nernst open-circuit voltage (V). V_{act} is the activation polarity loss (V). V_{ohm} is the ohmic polarity loss (V). V_{con} is the concentration loss (V). The thermal power of the stack can be obtained using Equation (11):

$$P_{st,heat} = N_{cell} \cdot (V_{Nernst} - V_{FC}) \cdot I_{cell} \quad (11)$$

Where, $P_{st,heat}$ is the PEMFC stack heat generation (W). N_{cell} is the number of fuel cells (-). I_{cell} is the cell current (A). The parameters of PEMFC stack are listed in Table 2. The PEMFC stack model was validated against experimental results [47]. More details of the methodology and experimental validation were provided in [48]. PEMFC stack model takes air inlet temperature T_{in}, operating temperature T_{st} and current density I_{FCS_dem} etc. as inputs and calculates stack output voltage V_{fcp}, heat generation heat $P_{st,heat}$, stack power P_{stack}. The operating temperature is regulated within the range of 320-360K. The cooling system is modeled to simulate controlled variations of cooling water flow rate and inlet cooling water temperature to maintain the stack temperature.

Table 2: PEMFC parameters [48]

Parameter (unit)	Value
Number of fuel cells N_{cell} (-)	220
Stack maximum power $P_{sta,max}$ (kW)	30
Anode inlet gas pressure P_a (atm)	1.0
Cathode inlet gas pressure P_c (atm)	1.6
Intake air temperature T_{in} (K)	348
Active area A (cm^2)	260

2.4.2 Cooling system

Control of the stack temperature is vital for efficiency optimization, lifetime extension, and operational safety of the hybrid vehicle. The cooling system model is built to ensure extra fuel cell heat will be removed to stabilize the stack temperature. Fig. 4 presents the schematic diagram of the PEMFC stack and the proposed cooling system.

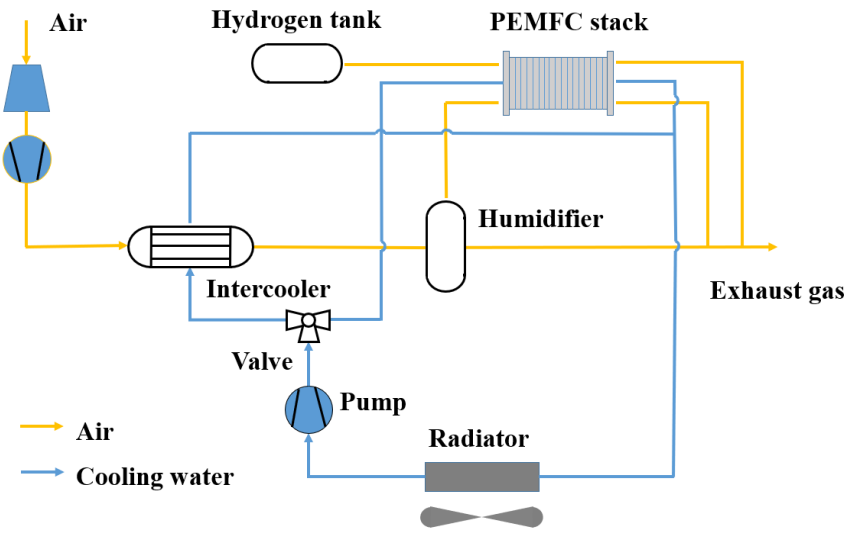

Figure 4: Schematic diagram of PEMFC stack and cooling system

Air is first compressed in the compressor; extreme high-temperature air will be cooled by the cooling water passing through the intercooler, humidified, then enter the cathode of the PEMFC stack. In the water loop, low temperature circulating cooling water enters the fuel cell, exchanges heat with the fuel cell stack, and exits the fuel cell at high temperature. The stack outlet cooling water will be mixed with the high temperature circulating water out of the intercooler. The mixed water enters the air-cooled radiator in which rejects heat to the air. The exiting cooled water out of the radiator is pressurized by the water pump and sent to the fuel cell stack through a part of the three-way valve. Amount of the cooling water enters the intercooler to cool the stack inlet. Stack inlet cooling water temperature and cooling water flow rate are two key

parameters that decide the stack temperature.

2.5 Battery system

A simple battery model has been developed. The influence of temperature on battery performance (such as internal resistance R_i, open circuit voltage V_0 and SOC) is ignored. It is assumed that the battery works at a constant temperature, only the influence of gassing coefficient η is considered, the ampere-hour method is used. The SOC and the battery voltage V_i can be calculated using Equations (12) and (13):

$$\frac{dSOC}{dt} = \frac{\eta}{3600C} \cdot I \tag{12}$$

$$V_i = V_0 - R_i \cdot I \tag{13}$$

Where, V_0 is the open circuit voltage of the battery (V), R_i is the internal resistance (Ω). I is the operating current (A), this equals to the battery demand current I_{soc_dem} calculated from the energy control unit model.

2.6 DC/DC converter

A DC/DC converter converts the input DC power into a DC power with a controllable voltage or current required by the load. A steady-state model is proposed. One end of the DC/DC converter is connected to the battery system, and one end is connected to the DC bus. When the battery is discharging, the converter is in the boost mode. When the battery is charging, the converter is in the discharging mode. The voltage at the DC bus connection is determined by the output voltage of the fuel cell and the voltage generated by the brake feedback of the drive motor.

The DC/DC circuit in actual application has power loss due to its components; the efficiency will change with the dynamic changes of the system; it is also different in

Buck mode and Boost mode. The relationship between current and voltage is as shown in Equations (14) and (15):

$$\text{Charge mode:} \quad I_{hvp\_lv} = \frac{V_{fcp} \cdot I_{hvp\_hv}}{V_{ebp} \cdot \eta_{boost}} \tag{14}$$

$$\text{Discharge mode:} \quad I_{hvp\_lv} = \frac{V_{fcp} \cdot I_{hvp\_hv} \cdot \eta_{buck}}{V_{ebp}} \tag{15}$$

Where, $I_{\text{hvp\_lv}}$ and $I_{\text{hvp\_hv}}$ (A)are the low-voltage end current and the high-voltage end current of the circuit respectively, V_{fcp} and V_{ebp} are the fuel cell voltage and power battery voltage (V). η_{boost} and η_{buck} are the circuit efficiency in boost and buck modes, respectively. The output of the model is the low voltage terminal current of the DC/DC circuit I_{hvp_lv}.

2.7 Motor model

The drive motor output torque acts directly on the drive wheels through the transmission components. Automobile motors need to be carefully selected due to their extensive range of torque, high efficiency, and strong stability and reliability. A permanent magnet brushless motor is chosen to establish the corresponding drive motor model. Equations (16) and (17) calculates the current demand for the motor for two different modes:

$$\text{Motor mode:} \quad I_m = \frac{\Gamma\omega_m + P_{motor\_loss}}{V} = \frac{\Gamma\omega_m + f(\omega_m, \Gamma)}{V} \tag{16}$$

$$\text{Generator mode:} \quad I_m = \frac{\Gamma\omega_m + P_{motor\_loss}}{V} = \frac{\Gamma\omega_m + f(\omega_m, -\Gamma)}{V} \tag{17}$$

Where, I_m is the current of the motor (A). Γ is the output torque of the motor (N·m). ω_m is the real-time speed of the motor calculated from the vehicle dynamic model (s^{-1}). P_{motor_loss} is the power loss of the motor (W), this parameter is a function of ω_m and Γ. V is the motor input voltage (V) from the DC/DC converter.

3 Results and discussions

3.1 PEMFC stack output current

Fig. 5 presents the PEMFC stack current under 674s driving cycles. The low-speed area of the Chinese passenger car driving curve presented in Fig. 3 is used as the input signal. The results show the at various vehicle speeds, the corresponding change curve of the fuel cell engine output current. In Fig. 5, when the car accelerates and the acceleration is high, the change of the output current at first follows the change of the vehicle speed. The PEMFC output current increases to around 40A, and the engine power consumption increases. When the car is driving at a constant speed or decelerating, the PEMFC output current is decreased to less than 10A, maintaining a minimum power value. When the vehicle speed is 0, the fuel cell is turned off, and the output current and power consumption become 0. Does the instant large stack current at the car acceleration impact the stack temperature and cause fuel cell degradation and a shorter life span? This will be analyzed and discussed in Section 3.2.

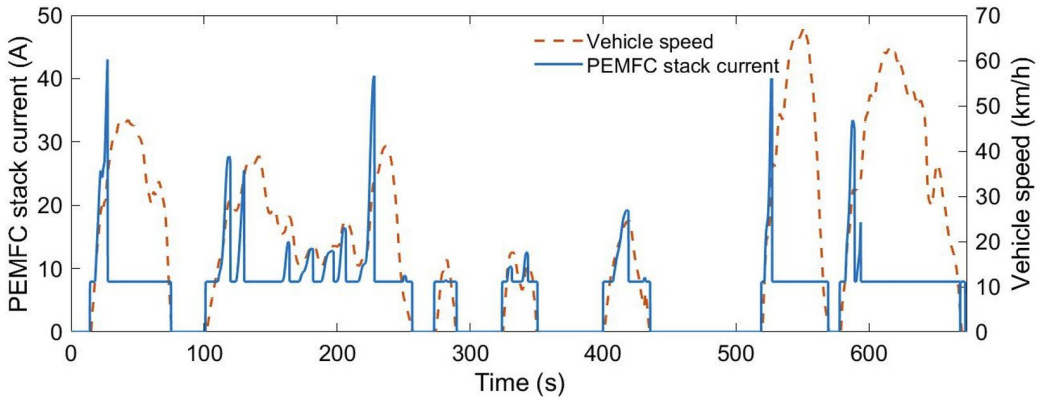

Figure 5: PEMFC stack current under driving cycles

3.2 Heat production and cooling performance

Fig. 6 shows the change curve of the fuel cell output power and heat generation power during the driving; the heat generation ratio at each driving condition are also calculated.

It is found that during the car's operation at low speed (0-65km/h), the ratio of stack-generated heat to the stack power ranges from 0.6-0.9. 33% to 50% of the total energy became stack heat and was dissipated to the air through the cooling system. The fuel cell generates high-efficiency electrical energy between 40% and 60% [49,50]. When the stack's power increases, the heat produced by the stack will also increase. The ratio of the generated heat to the stack power increases, and PEMFC engine efficiency decreases [51]. When the vehicle speed is relatively high, it is more necessary to pay attention to the heat dissipation of the PEMFC to maintain the operating temperature and ensure that the fuel cell works under the best operating conditions.

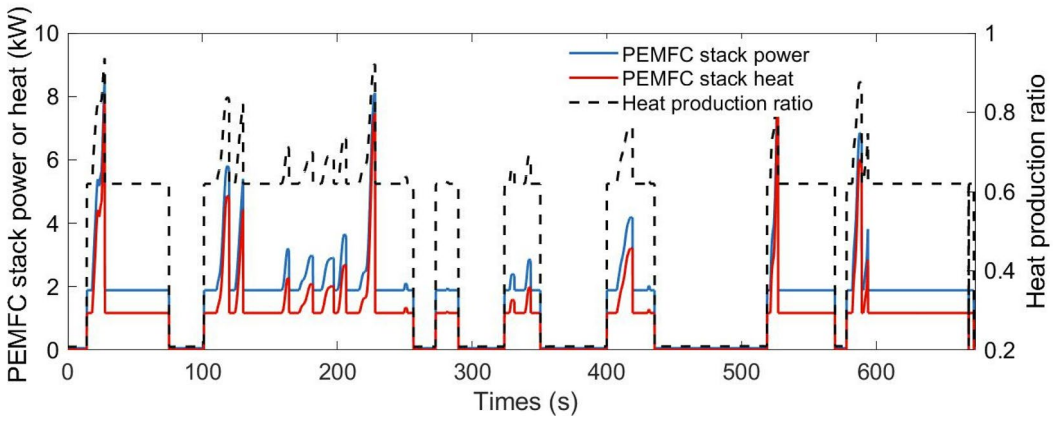

Figure 6: PEMFC stack power and heat generation

To understand the influence of the cooling water inlet temperature on the stack temperature, the inlet temperature is set to be 320K, 330K, 340K, 350K, 360K at cooling water flow rate 1kg/s. The initial stack temperature is set to 360K. Fig. 7 presents the changes in stack temperature under different inlet cooling water temperatures.

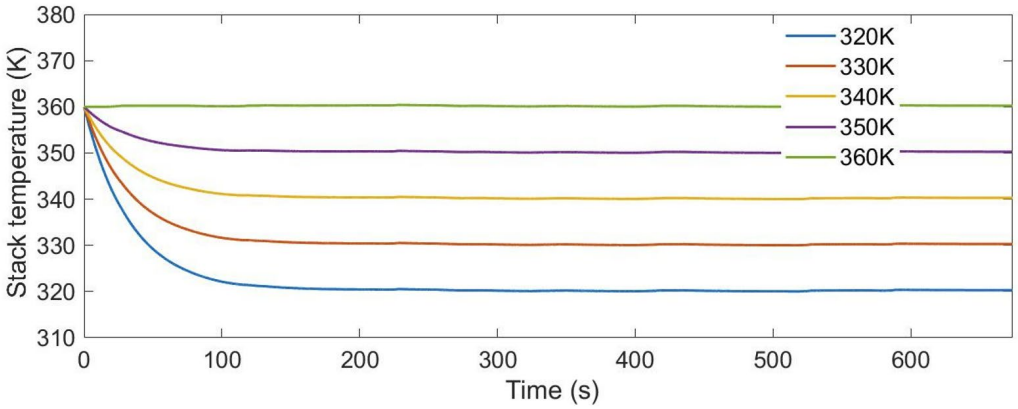

Figure 7: Inlet cooling water temperature and stack temperature

At the cooling water flow rate of 1kg/s, the stack temperature can almost reach the ideal equilibrium state. When the cooling water flow rate is large enough, the required time for each stack temperature curve to reach equilibrium is all similar, around 100s. The stack temperature is close to the inlet cooling water temperature in this case. To demonstrate the influence of the cooling water flow rate on the stack temperature variations, the flow rates are set as 0.2kg/s, 0.4 kg/s, 0.6kg/s, 0.8kg/s, 1.0kg/s, 2.0kg/s, and the inlet cooling water temperature is set to be constant at 350K. The simulation results are shown in Fig. 8. After 1 minute, when the cooling water flow rate varies from 0.2kg/s to 2kg/s, the stack temperature is 357.3K, 355.2K, 353.7K, 352.6K, 351.8K, 350.4K, respectively.

Figure 7 and Figure 8 both present the stack temperature when the coolant flow rate of 1kg/s and inlet temperature of 350K. Only focusing on stack temperature at the range of 350-360K, Fig. 8 can demonstrate the minor fluctuation of the stack temperature at actual driving conditions. The fluctuations in the stack temperature are caused by the occasional larger peak current and power of the fuel cell during the vehicle acceleration.

The heat generation increases and exceeds the cooling ability, the stack temperature transiently rises. Gradually, cooling water dissipate enough heat to reduce the stack temperature.

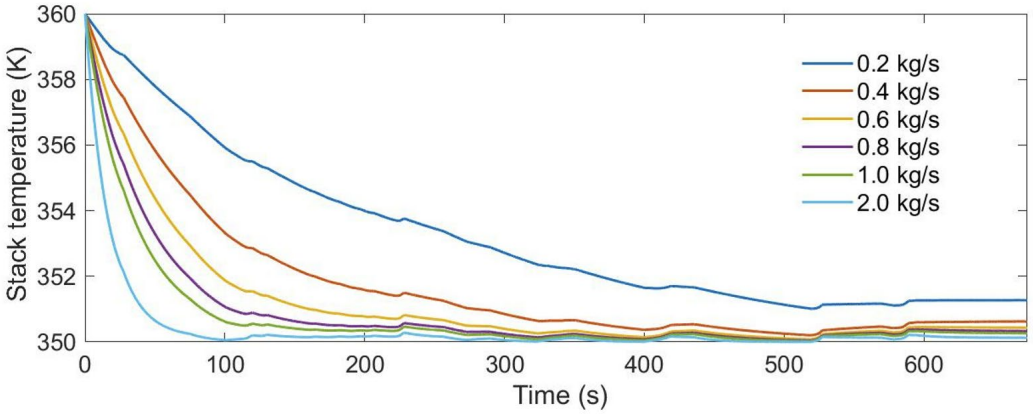

Figure 8: stack temperature in different cooling water flowrate

It can be found that under a water flow of 2kg/s, the stack temperature changes the fastest, the respond time is shorter [48]. The temperature drop at the water flow rate of 2kg/s is 9.6K, which is 3.56 times that of 0.2kg/s. The larger the water flow, the shorter time the stack temperature is to reach equilibrium; the water flow takes away more heat produced by the stack. At different cooling water flow rates, the steady-state stack temperatures are all in the range of 350-351K. Variation of the cooling water flow rate will not obviously impact the steady-state stack temperature. Moreover, when the stack is working, it is found that the occasional larger peak current and power due to the car acceleration will barely cause the stack temperature to fluctuate.

Although a more significant cooling flow rate will enhance the cooling performance, it may also bring the system control difficulties, unnecessary power consumption, and other shortcomings. The heat production and dissipation under driving conditions are

presented in Fig. 9. The cooling water inlet temperature is set to be 350K, at 1kg/s cooling water flow rate. The heat production of PEMFC varies with the output current. Soon after, the heat taken away by the cooling water rises and then decreases. This is because the peak current didn't last long; the amount of heat generated by the stack in a short period is limited. With cooling water flow rate and inlet cooling water temperature regulated appropriately, the heat dissipation requirements of the stack can be fully satisfied.

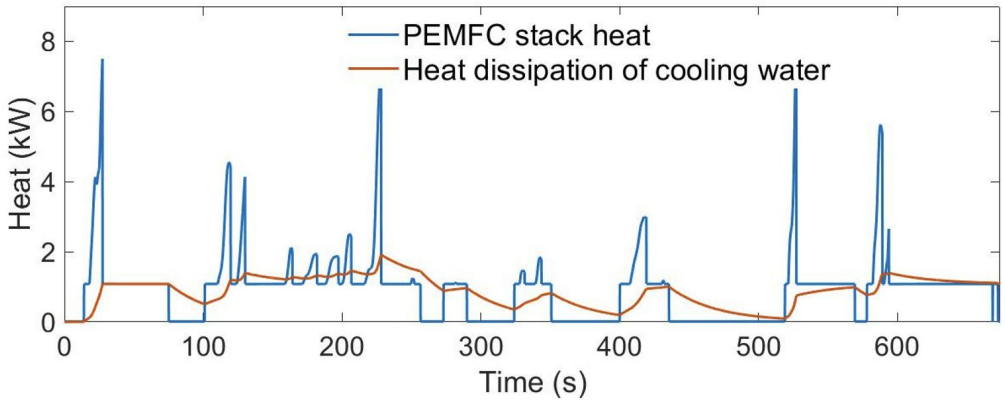

Figure 9: Comparison between PEMFC stack heat and cooling water heat

3.3 Thermal management – PID control

A PID controller is proposed for adjusting the cooling water flow rate and inlet cooling water temperature [41]. The control is to meet the heat dissipation requirement and to ensure the constant stack temperature. Varying of stack temperature under actual driving cycles may cause fuel cell degradation, which needs to be avoided [52]. The target stack temperature is set to be 350K. As discussed, and suggested in [48], the inlet cooling water temperature is constant; the cooling water flow rate will be regulated. Equations (18) and (19) presents the details of the PID control setting:

$$T_{st} - T_{inlet} = K_p \Delta T + K_i \int_0^t \Delta T dt + K_d \frac{d(\Delta T)}{dt} \quad (18)$$

$$\Delta T = T_{st} - T_{target} \quad (19)$$

Where, T_{st} is the stack temperature. T_{inlet} is the inlet cooling water temperature. T_{target} is the target stack temperature set to be 350K. K_p, K_i, K_d are respectively set to be 1, 1, 0. Fig. 10 (a) presents the stack temperature at different inlet cooling water temperatures (340K, 342K, 344K, 346K). In Fig. 10, it can be found that under the PID control strategy, the stack temperature will fluctuate up and down the target temperature of 350K. When the PEMFC power increases, the heat that the cooling water flow can take away is slightly less than the required heat dissipation, the stack temperature increases. The PID regulator starts to adjust the amount of cooling water to prevent the stack temperature from rising too fast. Once the PEMFC power stabilizes or drops, the stack temperature begins to decrease, changing toward the inlet cooling water temperature. This is because the cooling water flow matches the previous heat dissipation demand under high power. The low power situation will cause the heat dissipation to exceed the demand, so the PID regulator adjusts to reduce the flow rate and slow down the temperature drop.

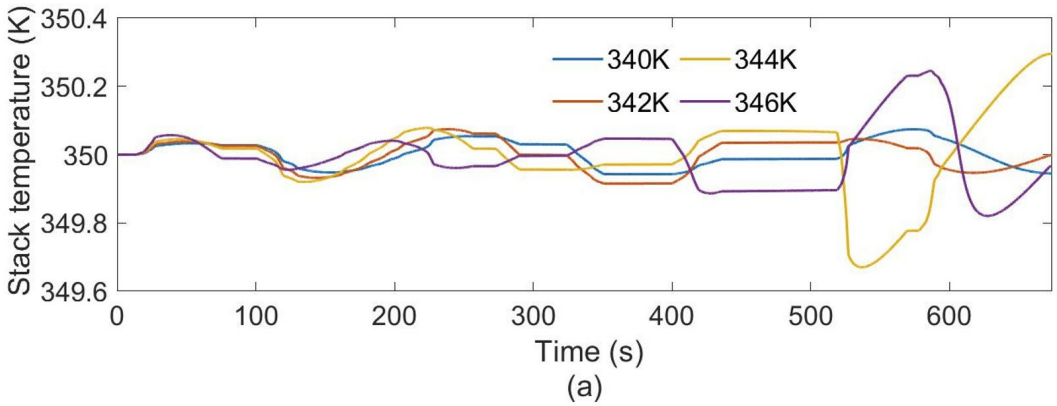

(a)

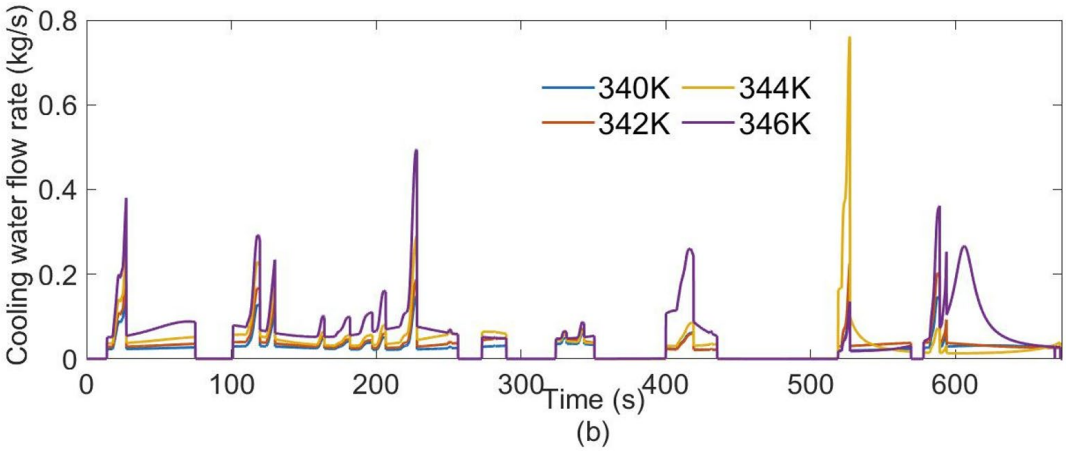

Figure 10: PID control of (a) stack temperature vs. inlet cooling water temperature (b) cooling water flow rate vas inlet cooling water temperature

On the other hand, the cooling water inlet temperature has an evident influence on the regulation effect. The difference between the second peak and trough of each curve is calculated. When the inlet cooling water temperature varies from 340K to 346K, the values are 0.10K, 0.19K, 0.23K, 0.38K. The maximum fluctuation amplitude is 3.67 times the minimum fluctuation amplitude. With the increase of inlet temperature, the oscillation frequency of the corresponding stack temperature becomes larger.

Fig. 10 (b) presents the cooling water flow rate variations at different inlet cooling water temperatures (340K, 342K, 344K, 346K). In general, the cooling water flow rate changes with FC stack heat production. Also, higher inlet cooling water temperature requires a larger cooling water flow rate. At the inlet temperature of 344K and 346K, the cooling water flow rate becomes unstable with the increase of the heat dissipation demand. A peak flow rate occurs when the inlet temperature is at 344K.

Overall, when the inlet cooling water temperature is small and the temperature difference with the target stack temperature (350K) is large, the fluctuation of the stack

temperature curve is obviously slowed down. When the inlet cooling water temperature increases and gets closer to the target stack temperature, the change of stack temperature becomes more significant; the adjustment becomes more and more difficult. This demonstrates that the lower cooling water inlet temperature to 340K improves the regulation ability of the PID control. However, lower cooling water inlet temperature also requires a higher fan and pumping power. Under actual driving cycles, considering the optimization of PID control performance and minimization of the fan and pump power, it is suggested to set a reasonable and constant value for the inlet cooling water temperature. Fig. 11 and Fig. 12 present the cooling water flow rate through the stack and the intercooler. The intercooler is used to cool the inlet compressed air.

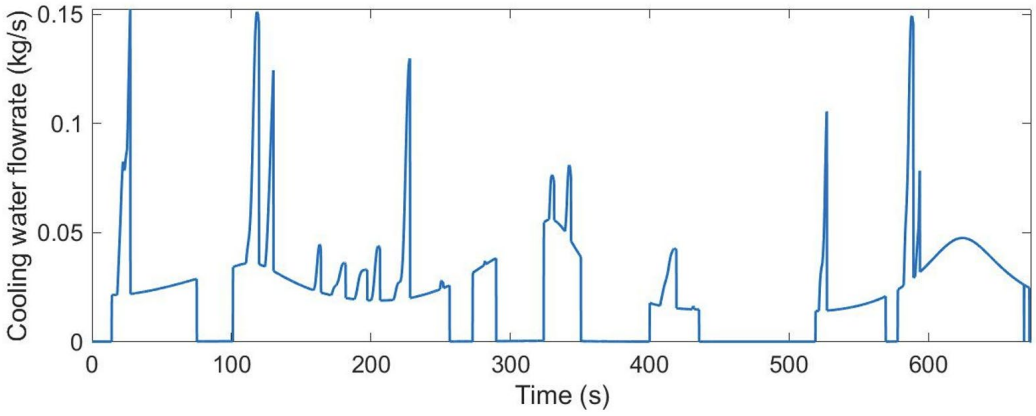

Figure 11: Cooling water flow through the PEMFC stack

The stack cooling water flow rate is two orders of magnitude higher than the intercooler cooling water flow rate. This shows that the heat dissipation requirement of the PEMFC stack is much higher than the heat dissipation requirement of the inlet compressed air. The cooling water flow change trend is quite similar to the stack output current and power trend. Promptly adjusting the cooling water flow rate using the PID control, the

cooling system of the PEMFC stack can meet the heat dissipation requirements under real driving cycles (0-65km/h).

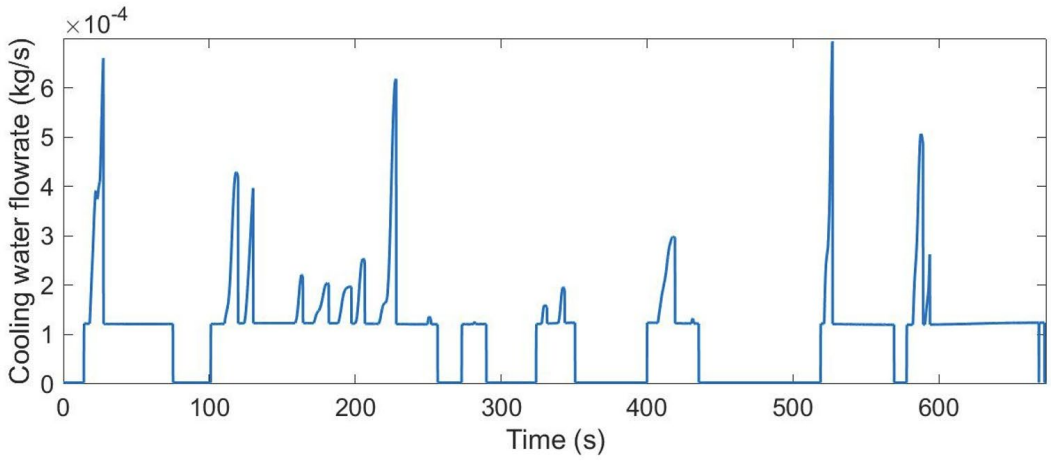

Figure 12: Cooling water through the intercooler

4 Conclusion

This paper presents a whole vehicle model for the fuel cell/battery hybrid vehicle to simulate the PEMFC stack performance under the actual driving cycles. A PID controller is proposed for the vehicle integrated thermal management. Under actual driving cycles (0-65kW/h), 33% to 50% of the total energy becomes stack heat and is dissipated through the cooling system. Promptly adjusting the cooling water flow rate using the PID control, the cooling system successfully stabilizes the stack temperature at 350K. Constant and relative lower inlet cooling water temperature (340K) improves the PID control regulation ability.

This paper presented the modeling of a fuel cell/battery hybrid fuel cell vehicle and its integrated thermal management system. The characteristics of the fuel cell stack under actual driving conditions were analyzed and discussed. There are few limitations of the conducted research; we suggest improving these in future work. Firstly, the battery's

temperature change and heat dissipation requirement were neglected; the dynamic characteristics of the motor were not considered. Secondly, the road conditions such as road surface material, slope, altitude, etc. had not been considered; the performance of vehicles in a harsh environment is worth further investigation. Thirdly, the fuel cell stack's performance at low-speed range of car driving conditions were analyzed; the performance at the middle and high-speed sections could be investigated later. Finally, a more effective and intelligent control strategy can be developed to enhance the vehicle's dynamic performance and ensure the fuel economy.

Acknowledgments

This work was supported by the National Key Research and Development Program of China, the National Natural Science Foundation of China (No. 51776144), Natural Science Foundation of Hubei Province (No. 2020CFA040) and Wuhan Applied Foundational Frontier Project (No. 2020010601012205).

References

[1] A. Alaswad, A. Baroutaji, H. Achour, J. Carton et al. Developments in fuel cell technologies in the transport sector. International Journal of Hydrogen Energy, 41(2016), pp. 16499-16509. https://doi.org/10.1016/j.ijhydene.2016.03.164.

[2] T. Willberforce, Z. EI-Hassan, F.N. Khatib, A.A. Makky et al. Developments of electric cars and fuel cell hydrogen delectric cars. International Journal of Hydrogen Energy, 42(2017), pp. 25695-25734. https://doi.org/10.1016/j.ijhydene.2017.07.054.

[3] B. Tanc B, H.T. Arat, E. Baltacioglu, K. Aydin. Overview of the next quarter century vision of hydrogen fuel cell electric vehicles. International Journal of Hydrogen

Energy, 44(2019), pp. 10120-10128. https://doi.org/10.1016/j.ijhydene.2018.10.112.

[4] Z. Dimitrova Z, W.B. Nader WB. PEM fuel cell as an auxiliary power unit for range extended hybrid electric vehicles. Energy, 239(2022), pp. 121933. https://doi.org/10.1016/j.energy.2021.121933.

[5] A. Baroutaji, A. Arjunan, M. Ramadan, J. Robinson et al. Advancements and propects of thermal management and waste heat recovery of PEMFC. International J. of Thermofluids, 9(2021), pp. 100064. https://doi.org/10.1016/j.ijft.2021.100064

[6] G.S. Zhang, S.G. Kandlikar. A critical review of cooling techniques in proton exchangemembrane fuel cell stacks. International Journal of Hydrogen Energy, 37(2012), pp. 2412-2429. https://doi.org/10.1016/j.ijhydene.2011.11.010.

[7] T. Lochner, R.M. Kluge, J. Fichtner, H.A. EI-Sayed, et al. Temperature effects in polymer electrolyte membrane fuel cell. ChemElectroChem, 7(2020), pp. 3545-3568. https://doi.org/10.1002/celc.202000588.

[8] J. Pharoah, O. Burheim. On the temperature distribution in polymer electrolyte fuel cells. Journal of Power Sources, 195(2010), pp. 5235-45. https://doi.org/10.1016/j.jpowsour.2010.03.024

[9] M.H.S. Bargal, M.A.A. Abdelkareem, Q. Tao, J. Li, et al. Liquid cooling techniques in proton exchangemembrane fuel cell stacks: A detailed survey. Alexandria Engineering Journal, 59(2020), pp. 635-655. https://doi.org/10.1016/j.aej.2020.02.005.

[10] W. Schmittinger, A. Vahidi. A review of the main parameters influencing long-termperformance and durability of PEM fuel cells. Journal of Power Sources, 180(2008), pp. 1-14. https://doi.org/10.1016/j.jpowsour.2008.01.070.

[11] M. Inci, M. Buyuk, M.H. Demir, G. Ilbey. A review and research on fuel cell electric vehicles: Topologies, power electronic converters, energy management methods, technical challenges, marketing and future aspects. Renewable and sustainable energy reviews, 137(2021), pp. 110648. https://doi.org/10.1016/j.rser.2020.110648.

[12] A. Faghri, Z. Guo. Challenges and opportunites of thermal management issues related to fuel cell technology and modeling. International J. of Heat and Mass Transfer, 48(2005), pp. 3891-3910. https://doi.org/10.1016/j.ijheatmasstransfer.2005.04.014.

[13] T. Zhang, P. Wang, H. Chen, P. Pei. A review of automotive proton exchange membrane fuel cell degradation under start-stop operating condition. Applied energy, 223(2018), pp. 249-62. https://doi.org/10.1016/j.apenergy.2018.04.049.

[14] J.C. Meier, C. Galeano, I. Katsounaros, A.A. Topalov, et al. Degradation mechanisms of Pt/C fuel cell catalysts under aimulated start−stop conditions. ACS Catal, 2(2012), pp. 832–843. https://doi.org/10.1021/cs300024h.

[15] E. Pahon, D. Bouquain, D. Hissel, A. Rouet, C. Vacquier. Performance analysis of proton exchange membrane fuel cell in automotive applications. J. of Power sources, 510(2021), pp. 230385. https://doi.org/10.1016/j.jpowsour.2021.230385

[16] A. Rabbani, M. Rokni, E. Hosseinzadeh, H.H. Mortensen. The start-up analysis of a PEM fuel cell system in vehicles. International Journal of Green Energy, 11(2014), pp. 91-111. https://doi.org/10.1080/15435075.2013.769882.

[17] S. Cheng, L. Xu, K. Wu, C. Fang, J. Hu, J. Li et al. Optimal warm-up control strategy of the PEMFC system on a city bus aimed at improving efficiency.

International Journal of Hydrogen Energy, 42(2017), pp. 11632-43. https://doi.org/10.1016/j.ijhydene.2017.02.203.

[18] Z.R. Yang, K. Jiao, K.C. Wu, W.L. Shi, et al. Numerical investigations of assisted heating cold start strategies for proton exchange membrane fuel cell systems. Energy, 222(2021), pp. 119910. https://doi.org/10.1016/j.energy.2021.119910.

[19] X.Q. Lü, Y.B. Wu, J. Lian, Y.Y. Zhang et al. Energy management of hybrid electric vehicles A review of energy optimization of fuel cell hybrid power system based on genetic algorithm. Energy conversion and Management, 205(2020), pp. 112474. https://doi.org/10.1016/j.enconman.2020.112474.

[20] Y. Zhou Y, A. Ravey A, M.C. Péra. Multi-objective energy management for fuel cell electric vehicles using online-learning enhanced Markov speed predictor. Energy Conversion Management, 213(2020), pp. 112821. https://doi.org/10.1016/j.enconman.2020.112821.

[21] W. Andari, S. Ghozzi, H. Allagui, A. Mami. Design, modeling and energy management of a PEM fuel cell/supercapacitor hybrid vehicle. International Journal of Advanced Computer Science Applications, 8(2017), pp. 273-8.

[22] Y. Wang, Z. Sun, Z. Chen. Energy management strategy for battery/supercapacitor/fuel cell hybrid source vehicles based on finite state machine. Appl. Energy, 254(2019), pp. 113707. https://doi.org/10.1016/j.apenergy.2019.113707.

[23] H. Zhang, X. Li, X. Liu, J. Yan. Enhancing fuel cell durability for fuel cell plug-in hybrid electric vehicles through strategic power management. Applied Energy. 21(2019), pp. 483-490. https://doi.org/10.1016/j.apenergy.2019.02.040.

[24] K. Kaya, Y. Hames. Two new control strategies: for hydrogen fuel saving and extend the life cycle in the hydrogen fuel cell vehicles. International J. of Hydrogen Energy. 44(2019), pp. 18697-18980. https://doi.org/10.1016/j.ijhydene.2018.12.111.

[25] T. Zeng, C.Z. Zhang, Y.Y. Zhang, C.H. Deng, et al. Optimization-oriented adaptive equivalent consumption minimization strategy based on short-term demand power prediction for fuel cell hybrid vehicle. Energy. 227(2021), pp. 120305. https://doi.org/10.1016/j.energy.2021.120305.

[26] Y.Z. Zhang, Z.Y. Huang, C.Z. Zhang, C. Lv, et al. Improved short-term speed prediction using spatiotemporal-vision-based deep neural network for intelligent fuel cell vehicles. IEEE Transactions on Industrial Informatics. 17(2021), pp. 6004-6013. 10.1109/TII.2020.3033980.

[27] M. Kandidayeni, A. Macias, L. Boulon, S. Kelouwani. Investigating the impact of ageing and thermal management of a fuel cell system on energy management strategies. Applied Energy, 274(2020), pp. 115293. https://doi.org/10.1016/j.apenergy.2020.115293.

[28] Y. Zhou, A. Ravey, M.C. Péra. Real-time cost-minimization power-allocating strategy via model predictive control for fuel cell hybrid electric vehicles. Energy Conversion Management, 229(2021), pp. 113271. https://doi.org/10.1016/j.enconman.2020.113721.

[29] H. Li, A. Ravey, A. N'Diaye, A. Djerdir. Online adaptive equivalent consumption minimization strategy for fuel cell hybrid electric vehicle considering power sources degradation. Energy Conversion and Management, 192(2019), pp. 133-

149. https://doi.org/10.1016/j.enconman.2019.03.090.

[30] Q. Li, Z. Liu, Y. Sun, S. Yang, C. Deng. A review on temperature control of proton exchange membrane fuel cells. Processes, 9(2021), pp. 235. https://doi.org/10.3390/pr9020235.

[31] V. Liso, M.P. Nielsen, S.K. Kær, H.H. Mortensen. Thermal modeling and temperature control of a PEM fuel cell system for forklift applications. International J. of hydrogen energy, 39(2014):8410-20. https://doi.org/10.1016/j.ijhydene.2014.03.175.

[32] M. Islam, B. Shabani, G. Rosengarten. Nanofluids to improve the performance of PEM fuel cell cooling systems: A theoretical approach. Applied Energy, 178(2016) , pp. 660-671. https://doi.org/10.1016/j.apenergy.2016.06.090.

[33] M.H.S. Bargal, M.M. Souby, M.A.A. Abdelkareem, M. Sayed et al. Experimental investigation of the thermal performance of a radiator using various nanofluids for automotive PEMFC applications. International Journal of Energy Research. 45(2020), pp. 6831-6849. https://doi.org/10.1002/er.6274.

[34] Q. Zhang, L. Xu, J. Li, M. Ouyang. Performance prediction of proton exchange membrane fuel cell engine thermal management system using 1D and 3D integrating numerical simulation. International Journal of Hydrogen Energy, 43(2018), pp. 1736-48. https://doi.org/10.1016/j.ijhydene.2017.10.088.

[35] J. Han, S. Yu. Ram air compensation analysis of fuel cell vehicle cooling system under driving modes. Applied Thermal Engineering, 142(2018), pp. 530-42. https://doi.org/10.1016/j.applthermaleng.2018.07.038.

[36] W. Sun, F.Y. Yi, D.H. Hu, J.M. Zhou. Research on matching design method of

waste heat reuse system of fuel cell vehicle considering system energy consumption and waste heat exchange rate. 45(2021), pp. 5470-5485. https://doi.org/10.1002/er.6175.

[37] K.F. Liang, M. Wang, C.Y. Gao, B. Dong, et al. Advances and challenges of integrated thermal management technologies for pure electric vehicles. Sustainable Energy Technologies and Assessments. 46(2021), pp. 101319. https://doi.org/10.1016/j.seta.2021.101319.

[38] P.Y. Lu, Q. Gao, L. Lv, X.Y. Xue, Y. Wang. Numerical calculation method of model predictive control for integrated vehicle thermal management based on underhood coupling thermal transmission. Energies. 12(2019), pp. 259. https://doi.org/10.3390/en12020259.

[39] Y.P. Wang, J. Li, Q. Tao, H.S.M. Bargal, et al. Thermal management system modeling and simulation of a full-power fuel cell vehicle. Energy resources technology. 142(2020), pp. 061304. https://doi.org/10.1115/1.4045479.

[40] Z. Zhao, T. Wang, B.F. Zhang, Y.Q. Wang, et al. Analysis of an integrated thermal management system with a heat-pump in a fuel cell vehicle. AIP Advance, 11(2021), pp. 065307. https://doi.org/10.1063/5.0056364.

[41] J.M. Xu, C.Z. Zhang, R.J. Fan, H.H. Bao, etc. Modeling and control of vehicle integrated thermal management system of PEM fuel cell vehicle. Energy. 199(2020), pp. 117495. https://doi.org/10.1016/j.energy.2020.117495.

[42] M. Ehsani, Y. Gao, S. Longo, K.M. Ebrahimi. Modern electric, hybrid electric, and fuel cell vehicles: fundamentals, theory, and design. CRC Press 2018. https://doi.org/10.1201/9780429504884.

[43] J. Bauman, M. Kazerani. A comparative study of fuel-cell–battery, fuel-cell–ultracapacitor, and fuel-cell–battery–ultracapacitor vehicles. IEEE Transactions on Vehicular Technology, 57(2008), pp. 760-9. 10.1109/TVT.2007.906379.

[44] S. Changizian, P. Ahmadi, M. Raeesi,N. Javani. Performance optimization of hybrid hydrogen fuel cell-electric vehicles in real driving cycles. Int. J. of Hydrogen Energy. 45(2020), pp. 35180-97. https://doi.org/10.1016/j.ijhydene.2020.01.015.

[45] S. Ma, M. Lin, T.E. Lin, T. Lan, et al. Fuel cell-battery hybrid systems for mobility and off-grid applications: A review. Renewable and Sustainable Energy Reviews. 135(2021), pp. 110119. https://doi.org/10.1016/j.rser.2020.110119.

[46] S. Zhou. Modeling and simulation technology of fuel cell vehicle. BeiJing, China. BeiJing Institute of Technology Press 2017.

[47] S. Chugh, C. Chaudhari, K. Sonkar, A. Sharma, et al. Experimental and modeling studies of low temperature PEMFC performance. Int. J. of Hydrogen Energy. 45(2020), pp. 8866-74. https://doi.org/10.1016/j.ijhydene.2020.01.019.

[48] L. Xing, H.W. Chang, R.Q. Zhu, T. Wang, Q.F. Zou, W.T. Xiang, Z.K. Tu. Thermal analysis and management of proton exchange membrane fuel cell stack for automotive vehicle. International Journal of Hydrogen Energy. 46(2021), pp. 32665-32675. https://doi.org/10.1016/j.ijhydene.2021.07.143.

[49] H.Q. Nguyen, B. Shabani. Proton exchange membrane fuel cells heat recovery opportunities for combined heating/cooling and power applications. Energy Convers. Manag, 204(2020), pp. 112328. https://doi.org/10.1016/j.enconman.2019.112328.

[50] N. Sazali, W.N.W. Salleh, A.S. Jamaludin, M.N.M. Razali. New perspectives

on fuel cell technology: a brief review. Membranes. 10(2020), pp. 99. https://doi.org/10.3390/membranes10050099.

[51] S. Pandiyan, K. Jayakumar, N. Rajalakshmi, K.S. Dhathathreyan. Thermal and electrical energy management in a PEMFCstack – An analytical approach. International Journal of Heat and Mass Transfer, 51(2008), pp. 469-473. https://doi.org/10.1016/j.ijheatmasstransfer.2007.05.024.

[52] L. Vichard, R. Petrone, F. Harel, A. Ravey. et al. Long term durability test of open-cathode fuel cell system under actualoperating conditions. Energy Convers. Manag., 212(2020), pp. 112813. https://doi.org/10.1016/j.enconman.2020.112813.